Identification of Mitochondrial Dysfunction in Hutchinson-Gilford Progeria Syndrome Through Use of Stable Isotope Labelling with Amino Acids in Cell Culture

José Rivera-Torres[1,*,†]; Rebeca Acín-Perez[2,*]; Pablo Cabezas-Sánchez[3,*]; Fernando G. Osorio[4]; Cristina Gonzalez-Gómez[1]; Diego Megias[5]; Carmen Cámara[3]; Carlos López-Otín[4]; José Antonio Enríquez[2]; José L. Luque-García[3] and Vicente Andrés[1,†]

[1] Department of Epidemiology, Atherothrombosis and Imaging, and [2] Department of Cardiovascular Development and Repair. Centro Nacional de Investigaciones Cardiovasculares (CNIC). Madrid. Spain.

[3] Department of Analytical Chemistry. School of Chemical Sciences. Complutense University of Madrid. Madrid. Spain.

[4] Departamento de Bioquímica y Biología Molecular, Instituto Universitario de Oncología (IUOPA). Universidad de Oviedo. Oviedo. Spain.

[5] Confocal Microscopy Unit. Centro Nacional de Investigaciones Oncológicas (CNIO). Madrid. Spain

* These authors contributed equally to this work.

† Corresponding authors:

Vicente Andrés (vandres@cnic.es)

José Rivera (jrivera@cnic.es)

CNIC

Melchor Fernández Almagro 3, 20029. Madrid. Spain.

Running Title: Mitochondrial dysfunction in progeria

Abbreviations

ATP5C1, ATP synthase, H+ transporting, mitochondrial F1 complex, gamma polypeptide
ATP5O, ATP synthase, H+ transporting, mitochondrial F1 complex, O subunit
ATP5B, ATP synthase, H+ transporting, mitochondrial F1 complex, beta polypeptide
ATP5A1, ATP synthase, H+ transporting, mitochondrial F1 complex, alpha subunit 1
ATP5F1, ATP synthase, H+ transporting, mitochondrial Fo complex, subunit B1
COX, cytochrome c oxidase
CS, citrate synthase
eIF2, eukaryotic translation initiation factor 2
eIF4, eukaryotic translation initiation factor 4
ENO2, enolase 2
FpSDH, flavoprotein subunit of succinate dehydrogenase
FTI, farnesyltransferase inhibitor
HGPS, Hutchinson-Gilford progeria syndrome
MAF, mouse adult fibroblast
mTOR, mammalian target of rapamycin
OXPHOS, oxidative phosphorylation
PKM, pyruvate kinase, muscle
p70S6K, ribosomal protein S6 kinase, 70kDa, polypeptide 1
SILAC, stable isotope labeling with amino acids in cell culture
Zmpste24, zinc metalloproteinase STE24 homolog

Abstract

Hutchinson-Gilford progeria syndrome (HGPS) is a rare segmental premature aging disorder that recapitulates some biological and physical aspects of physiological aging. The disease is caused by a sporadic dominant mutation in the *LMNA* gene that leads to the expression of progerin, a mutant form of lamin A that lacks 50 amino acids and retains a toxic farnesyl modification in its carboxy-terminus. However, the mechanisms underlying cellular damage and senescence and accelerated aging in HGPS are incompletely understood. Here, we analyzed fibroblasts from healthy subjects and HGPS patients using SILAC (stable isotope labeling with amino acids in cell culture). We found in HGPS cells a marked downregulation of mitochondrial oxidative phosphorylation proteins accompanied by mitochondrial dysfunction, a process thought to provoke broad organ decline during normal aging. We also found mitochondrial dysfunction in fibroblasts from adult progeroid mice expressing progerin (*Lmna*$^{G609G/G609G}$ knock-in mice) or prelamin A (*Zmpste24*-null mice). Analysis of tissues from these mouse models revealed that the damaging effect of these proteins on mitochondrial function is time- and dose-dependent. Mitochondrial alterations were not observed in brain, a tissue with extremely low progerin expression that seems to be unaffected in HGPS. Remarkably, mitochondrial function was restored in progeroid mouse fibroblasts treated with the isoprenylation inhibitors FTI-277 or pravastatin plus zoledronate, which are being tested in HGPS clinical trials. Our results suggest that mitochondrial dysfunction contributes to premature organ decline and aging in HGPS. Beyond its effects on progeria, prelamin A and progerin may also contribute to mitochondrial dysfunction and organ damage during normal aging, since these proteins are expressed in cells and tissues from non-HGPS individuals, most prominently at advanced ages.

Introduction

Nuclear lamins are type V intermediate filaments located beneath the inner nuclear membrane that provide structural support to the cell and play key roles in chromatin organization and gene expression [1, 2]. Three lamin genes have been identified in mammals [3]. *LMNA* encodes the alternatively spliced products lamin A and C (A-type lamins), which are expressed in most differentiated somatic cells, while *LMNB1* and *LMNB2* encode B-type lamins, which are expressed in nearly all cells and are essential for cell viability. Except for lamin C, nuclear lamins have a C-terminal CAAX motif (C, cysteine; A, aromatic amino acid; X, any residue) that is essential for protein maturation [4]. Post-translational modification of the CAAX motif comprises addition of a 15 carbon farnesyl lipid to the C residue followed by removal of the last three residues and finally methylation of the newly modified cysteine. Prelamin A undergoes a further maturation step consisting of removal of the last 15 amino acids by the zinc metalloproteinase ZMPSTE24/FACE-1, which produces mature lamin A [5].

Mutations in *LMNA* or defective processing of prelamin A cause a group of human diseases collectively called laminopathies, including the systemic disease known as Hutchinson-Gilford progeria syndrome (HGPS) [6-8]. The disease was first described in 1886 [9], but it was not until 2003 that its genetic basis was uncovered [10, 11]. Approximately 90% of HGPS patients have a non-inherited heterozygous synonymous mutation at codon 608 (c.1824C>T: GGC>GGT; p.G608G). This mutation activates the use of an internal 5' splice site in exon 11, which causes the deletion of 150 nucleotides and the synthesis of progerin (also named LAΔ50), a mutant form of prelamin A that lacks the ZMPSTE24 cleavage site and therefore retains a toxic farnesyl modification [10, 11]. Progerin, which exerts a dominant effect over the function of wild-type lamin A, causes structural abnormalities in the nuclear lamina, delays cytokinesis, hampers the DNA repair machinery and ultimately leads to the accumulation of DNA damage, increased genome instability and cell senescence [6]. Progerin accumulation might also contribute to physiological aging, since expression of this mutant form of prelamin A have been detected in cells from healthy individuals, predominantly at advanced ages [12-17]. Likewise, abnormal accumulation of prelamin A in arterial tissue might accelerate senescence of

vascular cells [18]. Telomere shortening and down-regulation of ZMPSTE24 during normal aging might contribute to progerin and prelamin A accumulation, respectively [17, 18]

Despite the importance of progerin and prelamin A in accelerated aging and their potential role in normal aging, our knowledge of the mechanisms through which these proteins cause cellular damage remains limited. To dissect the molecular mechanisms underlying HGPS, we performed a large-scale proteomic study based on stable isotope labeling with amino acids in cell culture (SILAC) and liquid chromatography in tandem with mass spectrometry (LC-MS/MS) to identify protein alterations in dermal fibroblasts from HGPS patients. Our proteomic analysis and functional studies in human HGPS cells and progeroid mouse models expressing progerin and prelamin A identify mitochondrial dysfunction as a hallmark of accelerated aging, a cellular alteration which is thought to contribute to physiological aging and age-associated pathologies [19-23]. We also show that mitochondrial defects in progeroid human and mouse cells are ameliorated by treatment with isoprenylation inhibitors.

EXPERIMENTAL PROCEDURES

Ethics Statement. All animal work has been conducted according to Directive 2010/63EU and Recommendation 2007/526/EC regarding the protection of animals used for experimental and other scientific purposes, enforced in Spanish law under Real Decreto 1201/2005.

Sample preparation for SILAC analysis. Primary skin fibroblasts from control subjects (GM01651, passage number 13 at purchase, from a healthy 13-year-old female; and GM08398, passage number 4 at purchase, from an 8-year-old male) and from HGPS patients carrying the typical c.1824C>T mutation (AG01972, passage number 12 at purchase, from a 14-year-old female; and AG06297,

passage number 19 at purchase, from an 8-year-old male) were obtained from the NIGMS Human Genetic Cell Repository (Coriell Institute). Figure 1 schematizes the study design. HGPS fibroblasts were grown asynchronously in 'light' ($^{12}C_6$-Lys and $^{12}C_6$-Arg) DMEM (Dundee Cell) supplemented with 10% FBS and 100 units/mL of penicillin/streptomycin for one round of duplication to achieve enough cell material. Control fibroblasts were grown asynchronously for at least six doublings (to ensure full incorporation of labeled amino acids) in 'heavy' ($^{13}C_6$-Lys and $^{13}C_6$-Arg) DMEM medium containing dialyzed FBS (Dundee Cell). After differential labeling, female and male HGPS cell lysates were prepared in RIPA buffer containing protease inhibitor cocktail (Roche) and mixed in a 1:1 ratio with the female and male control cell lysates, respectively. Mixtures were separated on 10% SDS-polyacrylamide gels, visualized by Coomassie blue staining, excised horizontally into 27 sections and further de-stained in 25mM ammonium bicarbonate/acetonitrile. De-stained bands were cut into smaller pieces, dehydrated with acetonitrile and dried, rehydrated with 12.5 ng/μl trypsin solution in 25 mM ammonium bicarbonate and incubated overnight at 37ºC. Digested peptides were extracted with acetonitrile and 5% formic acid, dried by vacuum centrifugation and reconstituted in 15 μl 2% acetonitrile in 0.1% formic acid. For both the male HGPS-control and female HGPS-control comparisons, two independent sets of lysates were mixed and processed as indicated above to provide a technical replicate.

MS and SILAC quantification. The peptide mixtures from the different in-gel digestion fractions were analyzed by nanoflow LC-MS/MS (Agilent Technologies). The peptides were loaded onto a 0.3 x 10mm C18 precolumn (SGE) and then eluted with a linear gradient of 5-95% ACN in a 0.1% aqueous solution of formic acid. The gradient was delivered over 120 min by a nano LC ultra 1D plus system (Eksigent) at a flow-rate of 200 nL/min, through a 75 μm x 15 cm fused silica capillary C18 HPLC PepMap column (LC Packings), to a stainless nano-bore emitter (Proxeon). The peptides were scanned and fragmented with an LTQ XL linear ion trap mass spectrometer (Thermo Finningan) operated in data-dependent ZoomScan and MS/MS switching mode using the three most intensive precursors detected in a survey scan from 400 to 1600 amu (three μscans). The ZoomScan mass

window was set to 12 Da, enabling monitoring of the entire $^{12}C/^{13}C$ isotopic envelope of most doubly and triply-charged peptides. Singly-charged ions were excluded from MS/MS analysis. Normalized collision energy was set to 35% and dynamic exclusion was applied during 3 min periods to avoid repetitive fragmentation of ions.

Generated raw files were converted to .mgf files (Bioworks 3.3.1) for submission to the MASCOT database. A database containing the NCBI nr *Homo sapiens* sequences (as of July 2009, 37391 sequences) was searched using the MASCOT protein identification software (v2.3 Matrix Science). Search criteria included trypsin specificity with one missed cleavage allowed, and with methionine oxidation, $^{13}C_6$-Arg and $^{13}C_6$–Lys as variable modifications. Minimum precursor and fragment-ion mass accuracies of 1.2 and 0.3 Da were used. To consider a protein as an accurate identification, at least one unique peptide (bold-red peptides meaning highest scoring peptide matching to protein with highest total score) with a Mascot score higher than 39 ($p<0.05$) and a minimum total protein score of 46 ($p<0.01$) were required. Peptide scores were derived from MS/MS data and total protein scores represent the sum of individual ion scores obtained on different peptides from the same protein. The false positive rate was calculated by searching the same spectra against the NCBI nr *Homo sapiens* decoy database. Relative quantification ratios of identified proteins based on peak area were calculated using Quixot v.1.3.26 open-source software (http://150.244.205.155/mediawiki/index.php/QuiXot). Protein ratios obtained by Quixot were verified manually for all peptides.

Mice. *Zmpste24*$^{-/-}$, *Lmna*$^{G609G/G609G}$ and *Lmna*$^{G609G/+}$ have been described previously [24, 25]. Homozygous *Zmpste24*$^{-/-}$ and *Lmna*$^{G609G/G609G}$ mice are infertile but seem healthy until about 3 weeks of age. Subsequently, they show a progressive reduction in body weight and size and appearance of aging symptoms leading to premature death (average life expectancy of 14-15 weeks compared to more than 2 years in wild-type controls). Heterozygous *Lmna*$^{G609G/+}$ mice have normal weight and size until about 8 months of age and then start to show aging symptoms and die at an average age of 34 weeks. Wild-type littermates with the *LMNA* gene intact were used as controls.

Generation of immortalized mouse fibroblasts. MAFs were isolated from the ears of 12-week-old wild-type, *Zmpste24*$^{-/-}$ and *Lmna*$^{G609G/G609G}$ mice as described previously [24]. Clumped cells were disrupted by pipetting and further filtered through a 45 μm cell strainer to obtain single cell suspensions. After 4-5 cell passages, primary MAFs were immortalized by retroviral transduction of SV40 large T antigen as described [26] and further maintained in high-glucose DMEM supplemented with 10% FBS.

Measurement of mitochondrial oxygen consumption, enzyme activities and ATP production. Pyruvate driven oxygen consumption rates (respiration) were measured in intact living cells ($2x10^6$ cells) at 37°C using an Oxytherm Electrode Unit equipped with a Clark electrode (Hansatech Instruments) [27]. Dinitrophenol was used to measure non-coupled respiration and values were expressed as nmol O_2 consumed per million cells per minute. COX activity was measured in cell lysates (30–50 μg protein) as described [28], and was normalized to the activity of CS, a Krebs cycle enzyme whose activity correlates with mitochondrial mass. ATP synthesis in digitonin-permeabilized cells ($2x10^6$) was measured using a kinetic luminescence assay as described [29].

Galactose/glucose growth assay. Immortalized MAFs ($1x10^4$) were seeded in 96-well plates and cultured for 4 days in DMEM containing either glucose (4.5 mg/ml) or galactose (0.9 mg/ml). Growth capacity was analyzed on a daily basis using the CyQUANT NF Cell proliferation assay kit (Invitrogen).

Cell treatments. MAFs were cultured for 7 days in growth medium with or without 5 μM FTI-277 (Sigma-Aldrich), or for 3 days with or without 5 μM pravastatine (Vasten; Sanofi Aventis) plus 5 μM zoledronate (ZOMETA, Novartis). In all cases, medium was replaced daily. After treatments, cells were washed with PBS and mitochondrial COX activity and ATP synthesis assays were carried our as indicated above.

186

187 ***Western blot.*** Mouse tissues were dissected, washed in PBS and immediately snap-frozen in liquid
188 nitrogen. Tissues were ground with a mortar and further homogenized with a Polytron tissue grinder.
189 Tissue and cell extracts were prepared in RIPA buffer supplemented with protease inhibitors (Roche).
190 Protein concentration was determined by the Bradford assay using BSA as standard (Protein Assay
191 Kit, Bio-Rad). Total protein extracts (50 μg) were mixed with Laemmli sample buffer (62.5 mMTris-
192 HCl, pH 6.8, 2.3% SDS, 10% glycerol, 5% β-mercaptoethanol, 0.005% bromophenol blue), boiled for
193 10 min and resolved on 10% SDS-polyacrylamide gels. Proteins were transferred to PVDF membranes
194 using the iBlot® Dry Blotting system (Invitrogen). The membranes were incubated for 1 h at room
195 temperature in blocking buffer (5% non-fat dried milk in TBS-0.2% Tween-20) followed by
196 incubation with primary antibodies diluted in blocking buffer (overnight, 4ºC). Primary antibodies
197 were purchased from Invitrogen (anti-FpSDH, ref. 459200; anti-COXI, ref. 459600), MitoSciences (β-
198 ATPase, ref. MS503), Sigma (Anti-actin, ref. A2066, anti-catalase, ref. CAT-505), Abcam (anti-
199 Cytochrome C, ref. ab13575), and Santa Cruz Biotech. (anti-Lamin A/C, ref. sc-6214). After washes
200 with TBS-0.2% Tween-20, membranes were incubated with HRP-conjugated secondary antibodies
201 (Santa Cruz) for 1 h at room temperature, and specific proteins were visualized by enhanced
202 chemiluminescence (GE Healthcare).

203

204 ***Statistical analyses.*** Results are presented as means±SD. The central hypothesis that is being tested in
205 this work is that progerin and prelamin A expression cause protein alterations and mitochondrial
206 dysfunction. Data were analyzed by unpaired two-tailed t-test (comparisons of two groups) or one-way
207 ANOVA with Dunnett's multiple comparison post-hoc test (experiments with more than two groups).
208 Differences were considered statistically significant at $p < 0.05$.

209

RESULTS

Proteome alterations in HGPS fibroblasts

To identify pathways altered in HGPS, we performed SILAC experiments to compare the proteomes of dermal fibroblasts from 1 female HGPS patient vs. 1 age-matched female healthy control and from 1 male HGPS patient vs. 1 age-matched male healthy control (Fig. 1). Each female [HGPS vs. control] and male [HGPS vs. control] sample set was processed and analysed twice, thus providing a technical replicate of each comparison (see Experimental Procedures). Complete incorporation of $^{13}C_6$-Arg and $^{13}C_6$-Lys into healthy fibroblasts after six doublings in isotopically heavy medium was verified by mass spectrometry (MS) of a protein digest (data not shown). Consistent with the observation that senescence is a characteristic of HGPS cells [6, 7], our HGPS fibroblasts grew very poorly and could be maintained in culture for a very limited time (data not shown). Therefore, we could not carry out reverse-incorporation of isotope labels.

MS analysis identified 3,304 proteins with at least one unique peptide in all four SILAC experiments and a false discovery rate of 0.6%, estimated from the number of hits against the reverse sequence/total hits ratio, $p<0.01$. However, only 819 and 720 proteins in male and female HGPS versus control comparisons, respectively, passed the criteria established for protein quantification, which include identification in at least two replicates of a given comparison set (male [HGPS vs. control] or female [HGPS vs. control]) and identification of at least two unique peptides with a MASCOT score >39 for the peptides and >46 for the full protein (see Supplemental Tables S1 and S2 showing proteins identified in the male and female comparisons, respectively). The global overlap between the four SILAC experiments was 48%. We then focused on proteins with at least a 1.5-fold difference between control and HGPS and with 20% as the maximum relative standard deviation between peptides within each protein. Most of the identified proteins had a SILAC ratio close to 1.

Amongst the 536 proteins showing ≥1.5 fold change and $p<0.01$ in both replicates of each female HGPS-control and male HGPS-control pool, we focused our attention on the 106 proteins that were significantly de-regulated in both the male and the female comparisons (26 expressed at higher level in HGPS: Supplemental Table S3 and 80 expressed at lower level in HGPS: Supplemental Table S4), since they are more likely to be a *bona fide* signature of altered progerin expression associated to HGPS. Proteins expressed at higher level in both male and female HGPS cells included proteins involved in glycolysis (PGK1, ENO2, PKM, and LDH), and those expressed at lower level included proteins of the translational apparatus (ribosomal proteins, eIF2, eIF4) and the mitochondrial oxidative phosphorylation system (OXPHOS) (proteins of ATP synthase complex V: ATP5C1, ATP5O, ATP5B, ATP5A1 and ATP5F1) (Fig. 2A).

Human HGPS fibroblasts exhibit mitochondrial dysfunction

Our proteomic analysis suggested that HGPS fibroblasts have profound metabolic alterations suggesting a metabolic switch from oxidative to glycolytic metabolism associated to defective OXPHOS. Accordingly, western blot analysis revealed markedly lower than normal expression of three crucial components of the mitochondrial respiratory chain in HGPS compared with control fibroblasts, including cytochrome c, the complex IV component cytochrome c oxidase subunit I (COXI), and the complex V protein β-ATPase (Fig. 2B). In contrast, we found no significant changes in the expression of succinate dehydrogenase flavoprotein, one of the four components of respiratory chain complex II, or of ubiquitously-expressed actin and catalase (Fig. 2B). These results demonstrate that HGPS fibroblasts have alterations in specific components localized both in the mitochondrial inner membrane (COXI) and the inter-membrane space (cytochrome c).

We next performed functional assays to directly assess mitochondrial function in HGPS and control fibroblasts. Analysis of pyruvate plus malate-driven mitochondrial ATP production revealed significantly lower ATP synthesis in progeroid fibroblasts (Fig. 2C)**.** Moreover, consistent with the western blot analysis, the activity of COX relative to that of citrate synthase (CS, typically used to normalize COX activity) was significantly lower in HGPS cells, with a COX/CS ratio 3-fold lower

than in control cells (Fig. 2D). These results demonstrate that OXPHOS is severely impaired in human HGPS fibroblasts.

Fibroblasts from progeroid Lmna$^{G609G/G609G}$ mice exhibit mitochondrial dysfunction

We next investigated whether the OXPHOS dysfunction observed in primary HGPS fibroblasts also occurs in the *Lmna$^{G609G/G609G}$* knock-in mouse model of the disease. These mice bear the *LMNA* c.1827C>T (p.G609G) mutation, equivalent to human c.1824C>T (p.G608G), express progerin as a consequence of aberrant exon11-12 *LMNA* splicing, and phenocopy the main clinical manifestations of human HGPS, including premature death [25]. Immortalized mouse adult fibroblasts (MAFs) derived from *Lmna$^{G609G/G609G}$* mice showed a significantly lower mitochondrial ATP synthesis than wild-type control fibroblasts (Fig. 3A)**.** Moreover, COX activity was significantly lower in *Lmna$^{G609G/G609G}$* fibroblasts, while CS activity was unaffected (Fig. 3B)**.** We also analyzed the functional state of the respiratory chain by measuring pyruvate-driven oxygen consumption in intact living cells. This analysis demonstrated that coupled and uncoupled respiration rates are both lower in *Lmna$^{G609G/G609G}$* MAFs than in wild-type controls (Fig. 3C)**.**

Changing the carbon source of the culture medium from glucose to galactose shuts down glycolysis, forcing cells to meet energy demand exclusively via OXPHOS. Cells with a defective OXPHOS system will therefore be unable to adapt their metabolism in galactose medium and will thus grow more slowly [30]. Culture in galactose-containing medium over four days revealed slow growth of progeroid *Lmna$^{G609G/G609G}$* MAFs compared with wild-type controls (Fig. 3D), confirming defective mitochondrial function in progeroid *Lmna$^{G609G/G609G}$* MAFs.

Mitochondrial dysfunction in tissues of Lmna$^{G609G/G609G}$ mice

We next analysed the consequences of progerin expression in tissues from wild-type and progeroid mice. High progerin expression has been reported in several tissues of homozygous *Lmna$^{G609G/G609G}$* mice compared with *Lmna$^{G609G/+}$* heterozygotes, including heart [31]. We found significantly lower

COX/CS ratios in the hearts of 10-week-old homozygous *Lmna*$^{G609G/G609G}$ and heterozygous *Lmna*$^{G609G/+}$ mice compared with wild-type littermates, an effect more pronounced in the homozygous progeroid mice (Fig. 4A)**.** The COX/CS ratio also decreased with age, being lower in the hearts of 32-week-old *Lmna*$^{G609G/+}$ mice compared with 10-week-old *Lmna*$^{G609G/+}$ mice (Fig. 4A). In 17-19-week-old *Lmna*$^{G609G/G609G}$ mice we also detected a low COX/CS ratio in skeletal muscle, another tissue expressing high levels of progerin (Fig. 4B, left) [31]. These studies thus indicate that the deleterious effects of progerin on mitochondrial function are time- and dose-dependent.

Recent studies have shown extremely low levels of prelamin A, lamin A and progerin in mouse and human neural cells [32, 33], which might explain why HGPS mouse models and patients seem to be free of pathology in the central nervous system. Consistent with these findings, progerin expression in the brains of 17-19-week-old *Lmna*$^{G609G/G609G}$ mice was extremely low, and this tissue showed no mitochondrial dysfunction in comparison with wild-type controls, as indicated by similar COX/CS ratios (Fig. 4B, right).

Expression of prelamin A in progeroid mice lacking Zmpste24 is associated with mitochondrial dysfunction

Loss of ZMPSTE24/FACE-1, the zinc metalloproteinase responsible for the final maturation of lamin A, causes the accumulation of prelamin A and lethal neonatal progeria in humans [34, 35]. Likewise, mice defective for Zmpste24 (*Zmpste24*$^{-/-}$) accumulate permanently farnesylated prelamin A and display an accelerated aging phenotype [5, 24]. We also found mitochondrial dysfunction in MAFs isolated from *Zmpste24*$^{-/-}$ mice, as revealed by significantly lower-than-wild-type ATP synthesis (Fig. 3A), COX/CS ratio (Fig. 3B), and coupled and uncoupled oxygen consumption (Fig. 3C), as well as impaired growth in galactose-containing medium (Fig. 3D). Furthermore, analysis of complex IV activity in *Zmpste24*$^{-/-}$ tissues confirmed the results obtained in *Lmna*$^{G609G/G609G}$ mice, with COX/CS ratios diminished in skeletal muscle (Fig. 4B) and heart (Fig. 4C), but with no effect in brain (Fig. 4B).

315 ***Isoprenylation inhibitors rescue ATP synthesis and COX activity in progeroid fibroblasts***

316 Expression of permanently farnesylated prelamin A or progerin leads to aberrant nuclear morphology,
317 a hallmark of HGPS. Treatment with farnesyl transferase inhibitors (FTIs) has demonstrated
318 therapeutic efficacy both in HGPS cells and in progeroid mice [36-39]. Recently, the results of a
319 clinical trial have provided preliminary evidence that the FTI lonafarnib may improve vascular
320 stiffness, bone structure and audiological status in HGPS patients [40]. We therefore investigated the
321 effect of FTI-277 on mitochondrial function in wild-type, *Zmpste24*$^{-/-}$ and *Lmna*$^{G609G/G609G}$ MAFs. Our
322 results demonstrate that FTI-277 significantly increases ATP synthesis and COX/CS ratio in
323 *Zmpste24*$^{-/-}$ and *Lmna*$^{G609G/G609G}$ MAFs, without affecting these parameters in wild-type cells (Fig. 5).

324 A combination of a statin (pravastatin) plus an aminobisphosphonate (zoledronate) also inhibits
325 isoprenylation of progerin and extends longevity in *Zmpste24*$^{-/-}$ mice [38]. Accordingly, ongoing Phase
326 II clinical trials are assessing the efficacy of this combined treatment
327 (http://www.progeriaresearch.org/clinical_trial.html, http://www.clinicaltrial.gov). Similarly to the
328 treatment with FTI-277, addition of pravastatin+zoledronate to the culture medium did not affect the
329 mitochondrial performance of wild-type MAFs, but significantly improved ATP synthesis and
330 COX/CS ratio in *Zmpste24*$^{-/-}$ and *Lmna*$^{G609G/G609G}$ progeroid MAFs (Fig. 5).

331

332

DISCUSSION

To unravel the molecular mechanisms involved in HGPS, we performed unbiased proteomic analysis and functional assays in cellular and mouse models expressing progerin, the lamin A mutant protein responsible for this premature aging syndrome. Our SILAC analysis using human dermal fibroblasts from HGPS patients and age-matched healthy controls allowed the identification and quantification of 3,304 proteins, of which 536 were differentially regulated after applying very stringent criteria for selection (175 up-regulated and 361 down-regulated in HGPS). These results represent a significant advance in comparison with previous studies that reported only 7 [41] and 30 [42] altered proteins in HGPS fibroblasts. In agreement with these previous studies, we found alterations in α-actinin, vimentin, several annexin isoforms, tropomyosin α-4, protein disulfide-isomerase, elongation factor 1, ribosomal protein L6, SNX3, galectin1 and hsp90, among others. It is important to note that our SILAC results have to be interpreted as an overall protein dysregulation profile in HGPS fibroblasts, which is likely to result from a mixture of damaging and compensation effects. Future studies are therefore required to unravel the hierarchy of protein alterations in HGPS. Of note, although we only performed SILAC in fibroblasts from one male and one female patient and age- and gender-matched controls, we focused our functional analysis in proteins involved in OXPHOS which exhibited statistically significant differences in both gender comparisons, since they are more likely to be a *bona fide* signature of altered progerin expression associated to HGPS. Indeed, we corroborated by western blot and functional assays the reduction in OXPHOS proteins and mitochondrial dysfunction in both male and female human HGPS fibroblasts, thus demonstrating the consistency of our SILAC studies.

It is increasingly evident that A-type lamins play important roles in gene regulation [1]. Our SILAC results showed that more than 65% of the differentially regulated proteins are down-regulated in HGPS fibroblasts expressing progerin. These included proteins of the mTOR pathway, which positively regulates the activity of factors involved in protein translation [43]. Consistent with this, the largest cluster of down-regulated proteins in HGPS fibroblasts are key components of the translational apparatus, including 28 ribosomal proteins, 6 translation initiation factors and 3 translation elongation factors. Moreover, we found a 2-fold down-regulation of the mTOR target CD44. These findings in

human cells reinforce previous data from progeroid *Zmpste24*$^{-/-}$ mice, which showed impaired mTOR signaling [44]. Despite the fact that progeria leads to mTOR inhibition, it was recently reported that treatment of HGPS cells with the mTOR inhibitor rapamycin promotes proteasomal progerin degradation, prevents nuclear abnormalities and delays the onset of cellular senescence [45]. Further studies are thus warranted to explain this apparent paradox and to investigate the functional consequences of the observed alterations in key components of translational apparatus, including ribosomal proteins, translational initiation factors and translation elongation factors.

We also found that HGPS fibroblasts exhibit lower level of proteins related to mitochondrial biology, including OXPHOS, mitochondrial dysfunction, and oxidative stress, and previous studies have shown higher levels of reactive oxygen species and oxidized protein in HGPS fibroblasts compared to age-matched controls [46]. Remarkably, mitochondrial dysfunction can lead to excessive oxidative stress, which in turn can aggravate mitochondrial dysfunction [19]. To our knowledge, the present study provides the first demonstration that HGPS is associated with reduced expression of key components of the mitochondrial OXPHOS pathway. Importantly, we find that these alterations are accompanied by diminished oxidative phosphorylation capacity, as revealed by a marked reduction in the activity of mitochondrial complex IV (COX/CS, >65%) and the rate of mitochondrial ATP synthesis (~50%) compared with age-matched healthy controls. Extending the relevance of these findings, our examination of fibroblasts from progeroid *Lmna*$^{G609G/G609G}$ mice expressing progerin also revealed reduced mitochondrial ATP synthesis, COX/CS ratio and oxygen consumption (a measure of overall respiratory chain activity), and an impaired capacity to grow in galactose-containing medium. Likewise, we found mitochondrial alterations in fibroblasts from *Zmpste24*$^{-/-}$ mice that accumulate high levels of prelamin A, which also causes premature aging in humans and mice [24, 34, 35]. Accordingly, tissues from *Lmna*$^{G609G/G609G}$ and *Zmpste24*$^{-/-}$ mice show mitochondrial alterations, revealed by impaired COX/CS ratio and mitochondrial ATP synthesis. Our results indicate that the effects of progerin are dose- and time-dependent, since analysis of protein lysates from heart tissue revealed more pronounced mitochondrial dysfunction in 10-week-old homozygous *Lmna*$^{G609G/G609G}$ versus heterozygous *Lmna*$^{G609G/+}$ mice, and in old (32-week-old) versus young (10-week-old)

388 *Lmna*$^{G609G/+}$ mice. In agreement with the present results, we recently demonstrated mitochondrial
389 dysfunction in vascular smooth muscle cells from *Lmna*$^{G609G/+}$ mice [47]. Taken together, these
390 findings underscore mitochondrial dysfunction as a general feature of progeroid syndromes caused by
391 abnormal expression of either progerin or prelamin A. Interestingly, up-regulated proteins in HGPS
392 included glycolytic enzymes (PGK1, ENO2, PKM) and lactate dehydrogenase, which are likely to
393 compensate the decrease in mitochondrial ATP production caused by progerin or prelamin A
394 expression. Indeed, mitochondrial dysfunction has been associated with different human pathologies,
395 including neurodegenerative diseases, cancer, diabetes and cardiovascular disease [48]. Remarkably,
396 impaired mitochondrial activity has been reported in HIV-treated patients displaying lipodystrophy
397 [49], one of the main alterations shared by progeroid mouse models and HGPS patients. It is
398 noteworthy that adipose tissue dysfunction in *Zmpste24*$^{-/-}$ mice is associated with up-regulation of
399 proteins involved in the tricarboxylic acid cycle and OXPHOS, enhanced lipolysis, fatty acid
400 biogenesis and β-oxidation, and low fatty acid re-esterification [50]. Additional work is thus warranted
401 to elucidate the molecular mechanisms underlying the tissue specificity of metabolic alterations and
402 mitochondrial dysfunction in premature aging syndromes. It would be also of interest to examine in
403 progeroid mice metabolic rates, respiratory quotient and oxygen consumption measurements at early
404 ages before symptoms develop as well as in animals with overt disease.

405 A large body of evidence suggests that defective mitochondrial function is a major factor
406 driving normal aging [19-23] that may also underlie progeroid manifestations in Polg mutator mice
407 [51]. Our results show that premature aging caused by progerin or prelamin A is associated with
408 defective mitochondrial function. Of note, recent studies have shown that miRNA-9 negatively
409 controls lamin A and progerin expression in neural cells [32, 33], which might explain why HGPS-like
410 mice and HGPS patients do not exhibit recognizable central nervous system abnormalities.
411 Remarkably, we find that progeroid *Zmpste24*$^{-/-}$ and *Lmna*$^{G609G/G609G}$ mice express very low levels of
412 prelamin A and progerin, respectively, in the brain, and in both models brain mitochondrial function is
413 normal. It is also noteworthy that telomere ablation, which occurs during normal aging and is thought
414 to impair cell and organismal homeostasis [22, 52, 53], has been shown to induce progerin expression

and cellular senescence in normal human fibroblasts [17], and is associated with mitochondrial dysfunction in mice lacking telomerase activity [54]. Moreover, fibroblasts from HGPS patients exhibit shorter telomeres than control cells [55, 56]. Therefore, telomere and mitochondrial dysfunction, which have been recently proposed to play a central role in normal aging [22, 54], may also contribute to premature aging caused by abnormal accumulation of prelamin A or progerin, a possibility that merits further investigation. It is also tempting to speculate that these proteins may worsen mitochondrial function and organ decline during normal aging, since they have been shown to accumulate in several cells and tissues in non-HGPS individuals, most prominently at advanced ages [12-18].

Tissue culture and animal studies have demonstrated that farnesylated progerin exerts a dominant negative effect and plays a major role in the etiopathogenesis of HGPS [6]. In line with this notion, inhibition of progerin isoprenylation improves the nuclear abnormalities and the aging-like phenotypes, both in progeroid cells and in mice [36-39]. Recently, the results from a clinical trial enrolling 25 children with HGPS who were treated with the FTI lonafarnib for at least 2 years revealed increased rate of weight gain and improved measures of vascular stiffness, bone structure or audiological status for some patients [40]. The efficacy of inhibiting progerin isoprenylation is being also evaluated in ongoing clinical trials using a combination of statins plus aminobisphosphonates (http://www.progeriaresearch.org/clinical_trial.html and http://www.clinicaltrial.gov). We find that these treatments restore mitochondrial function in progeroid *Lmna*$^{G609G/G609G}$ and *Zmpste24*$^{-/-}$ fibroblasts, as revealed by improved complex IV and V activities. Whether these drugs also ameliorate mitochondrial function in HGPS patients and in other mitochondrial diseases remains to be examined. Further studies are also needed to unravel the mechanisms through which farnesylated progerin and prelamin A provoke mitochondrial abnormalities, which may pave the way to improved treatments of HGPS. Given that these proteins accumulate during normal aging, these studies may also improve our knowledge of the mechanisms leading to mitochondrial dysfunction during normal aging.

Acknowledgements

We thank María Jesús Andrés for technical assistance and figure preparation, and Simon Bartlett for English editing. Work in the author's laboratories is supported by grants from the Spanish Ministry of Economy and Competiveness (MINECO) (SAF2010-16044; SAF2011-23089, SAF2009-08007, CSD2007-00020, CTQ2010-18644), Instituto de Salud Carlos III (ISCIII) (RD06/0014/0021, RD12/0042/0028), The Progeria Research Foundation (Innovator Award PRF 2012-42), and Comunidad de Madrid (S2011/BMD-2402). P.C.-S. was financially supported by an FPU scholarship from the Spanish Ministry of Education. The Centro Nacional de Investigaciones Cardiovasculares (CNIC) is supported by MINECO and Pro-CNIC Foundation, and the Instituto Universitario de Oncología by Obra Social Cajastur. The funders had no role in study design, data collection and analysis, decision to publish, or preparation of the manuscript.

455
456 **References**

457 [1] Andres V, Gonzalez JM. Role of A-type lamins in signaling, transcription, and chromatin
458 organization. J Cell Biol. 2009;187:945-57.
459 [2] Mekhail K, Moazed D. The nuclear envelope in genome organization, expression and
460 stability. Nature reviews Molecular cell biology. 2010;11:317-28.
461 [3] Dechat T, Adam SA, Taimen P, Shimi T, Goldman RD. Nuclear lamins. Cold Spring Harb
462 Perspect Biol. 2010;2:a000547.
463 [4] Trigueros-Motos L, Gonzalez JM, Rivera J, Andres V. Hutchinson-Gilford progeria
464 syndrome, cardiovascular disease and oxidative stress. Front Biosci (Schol Ed).
465 2011;3:1285-97.
466 [5] Pendas AM, Zhou Z, Cadinanos J, Freije JM, Wang J, Hultenby K, et al. Defective
467 prelamin A processing and muscular and adipocyte alterations in Zmpste24
468 metalloproteinase-deficient mice. Nat Genet. 2002;31:94-9.
469 [6] Broers JL, Ramaekers FC, Bonne G, Yaou RB, Hutchison CJ. Nuclear lamins:
470 laminopathies and their role in premature ageing. Physiol Rev. 2006;86:967-1008.
471 [7] Capell BC, Collins FS. Human laminopathies: nuclei gone genetically awry. Nat Rev
472 Genet. 2006;7:940-52.
473 [8] Gonzalez JM, Pla D, Perez-Sala D, Andres V. A-type lamins and Hutchinson-Gilford
474 progeria syndrome: pathogenesis and therapy. Front Biosci (Schol Ed). 2011;3:1133-46.
475 [9] Hutchinson J. Congenital Absence of Hair and Mammary Glands with Atrophic Condition
476 of the Skin and its Appendages, in a Boy whose Mother had been almost wholly Bald
477 from Alopecia Areata from the age of Six. Med Chir Trans. 1886;69:473-7.
478 [10] De Sandre-Giovannoli A, Bernard R, Cau P, Navarro C, Amiel J, Boccaccio I, et al.
479 Lamin a truncation in Hutchinson-Gilford progeria. Science. 2003;300:2055.
480 [11] Eriksson M, Brown WT, Gordon LB, Glynn MW, Singer J, Scott L, et al. Recurrent de
481 novo point mutations in lamin A cause Hutchinson-Gilford progeria syndrome. Nature.
482 2003;423:293-8.
483 [12] McClintock D, Ratner D, Lokuge M, Owens DM, Gordon LB, Collins FS, et al. The
484 mutant form of lamin A that causes Hutchinson-Gilford progeria is a biomarker of
485 cellular aging in human skin. PLoS One. 2007;2:e1269.
486 [13] Olive M, Harten I, Mitchell R, Beers JK, Djabali K, Cao K, et al. Cardiovascular
487 pathology in Hutchinson-Gilford progeria: correlation with the vascular pathology of
488 aging. Arterioscler Thromb Vasc Biol. 2010;30:2301-9.
489 [14] Scaffidi P, Misteli T. Lamin A-dependent nuclear defects in human aging. Science.
490 2006;312:1059-63.
491 [15] Cao K, Capell BC, Erdos MR, Djabali K, Collins FS. A lamin A protein isoform
492 overexpressed in Hutchinson-Gilford progeria syndrome interferes with mitosis in
493 progeria and normal cells. Proc Natl Acad Sci U S A. 2007;104:4949-54.
494 [16] Rodriguez S, Coppede F, Sagelius H, Eriksson M. Increased expression of the
495 Hutchinson-Gilford progeria syndrome truncated lamin A transcript during cell aging.
496 Eur J Hum Genet. 2009;17:928-37.
497 [17] Cao K, Blair CD, Faddah DA, Kieckhaefer JE, Olive M, Erdos MR, et al. Progerin and
498 telomere dysfunction collaborate to trigger cellular senescence in normal human
499 fibroblasts. J Clin Invest. 2011;121:2833-44.
500 [18] Ragnauth CD, Warren DT, Liu Y, McNair R, Tajsic T, Figg N, et al. Prelamin A acts to
501 accelerate smooth muscle cell senescence and is a novel biomarker of human vascular
502 aging. Circulation. 2010;121:2200-10.

[19] Lopez-Otin C, Blasco MA, Partridge L, Serrano M, Kroemer G. The hallmarks of aging. Cell. 2013;153:1194-217.
[20] Bratic A, Larsson NG. The role of mitochondria in aging. J Clin Invest. 2013;123:951-7.
[21] Galluzzi L, Kepp O, Trojel-Hansen C, Kroemer G. Mitochondrial control of cellular life, stress, and death. Circ Res. 2012;111:1198-207.
[22] Sahin E, DePinho RA. Axis of ageing: telomeres, p53 and mitochondria. Nature reviews Molecular cell biology. 2012;13:397-404.
[23] Wallace DC. A mitochondrial paradigm of metabolic and degenerative diseases, aging, and cancer: a dawn for evolutionary medicine. Annu Rev Genet. 2005;39:359-407.
[24] Varela I, Cadinanos J, Pendas AM, Gutierrez-Fernandez A, Folgueras AR, Sanchez LM, et al. Accelerated ageing in mice deficient in Zmpste24 protease is linked to p53 signalling activation. Nature. 2005;437:564-8.
[25] Osorio FG, Navarro CL, Cadinanos J, Lopez-Mejia IC, Quiros PM, Bartoli C, et al. Splicing-directed therapy in a new mouse model of human accelerated aging. Sci Transl Med. 2011;3:106ra7.
[26] Tevethia MJ, Ozer HL. SV40-mediated immortalization. Methods Mol Biol. 2001;165:185-99.
[27] Hofhaus G, Shakeley RM, Attardi G. Use of polarography to detect respiration defects in cell cultures. Methods Enzymol. 1996;264:476-83.
[28] Birch-Machin MA, Turnbull DM. Assaying mitochondrial respiratory complex activity in mitochondria isolated from human cells and tissues. Methods Cell Biol. 2001;65:97-117.
[29] Vives-Bauza C, Yang L, Manfredi G. Assay of mitochondrial ATP synthesis in animal cells and tissues. Methods Cell Biol. 2007;80:155-71.
[30] Enriquez JA, Cabezas-Herrera J, Bayona-Bafaluy MP, Attardi G. Very rare complementation between mitochondria carrying different mitochondrial DNA mutations points to intrinsic genetic autonomy of the organelles in cultured human cells. J Biol Chem. 2000;275:11207-15.
[31] Lopez-Mejia IC, Vautrot V, De Toledo M, Behm-Ansmant I, Bourgeois CF, Navarro CL, et al. A conserved splicing mechanism of the LMNA gene controls premature aging. Hum Mol Genet. 2011;20:4540-55.
[32] Nissan X, Blondel S, Navarro C, Maury Y, Denis C, Girard M, et al. Unique preservation of neural cells in Hutchinson- Gilford progeria syndrome is due to the expression of the neural-specific miR-9 microRNA. Cell Rep. 2012;2:1-9.
[33] Jung HJ, Coffinier C, Choe Y, Beigneux AP, Davies BS, Yang SH, et al. Regulation of prelamin A but not lamin C by miR-9, a brain-specific microRNA. Proc Natl Acad Sci U S A. 2012;109:E423-31.
[34] Navarro CL, Cadinanos J, De Sandre-Giovannoli A, Bernard R, Courrier S, Boccaccio I, et al. Loss of ZMPSTE24 (FACE-1) causes autosomal recessive restrictive dermopathy and accumulation of Lamin A precursors. Hum Mol Genet. 2005;14:1503-13.
[35] Navarro CL, De Sandre-Giovannoli A, Bernard R, Boccaccio I, Boyer A, Genevieve D, et al. Lamin A and ZMPSTE24 (FACE-1) defects cause nuclear disorganization and identify restrictive dermopathy as a lethal neonatal laminopathy. Hum Mol Genet. 2004;13:2493-503.
[36] Capell BC, Olive M, Erdos MR, Cao K, Faddah DA, Tavarez UL, et al. A farnesyltransferase inhibitor prevents both the onset and late progression of cardiovascular disease in a progeria mouse model. Proc Natl Acad Sci U S A. 2008;105:15902-7.

[37] Fong LG, Frost D, Meta M, Qiao X, Yang SH, Coffinier C, et al. A protein farnesyltransferase inhibitor ameliorates disease in a mouse model of progeria. Science. 2006;311:1621-3.
[38] Varela I, Pereira S, Ugalde AP, Navarro CL, Suarez MF, Cau P, et al. Combined treatment with statins and aminobisphosphonates extends longevity in a mouse model of human premature aging. Nat Med. 2008;14:767-72.
[39] Young SG, Meta M, Yang SH, Fong LG. Prelamin A farnesylation and progeroid syndromes. J Biol Chem. 2006;281:39741-5.
[40] Gordon LB, Kleinman ME, Miller DT, Neuberg DS, Giobbie-Hurder A, Gerhard-Herman M, et al. Clinical trial of a farnesyltransferase inhibitor in children with Hutchinson-Gilford progeria syndrome. Proc Natl Acad Sci U S A. 2012;109:16666-71.
[41] Robinson LJ, Karlsson NG, Weiss AS, Packer NH. Proteomic analysis of the genetic premature aging disease Hutchinson Gilford progeria syndrome reveals differential protein expression and glycosylation. J Proteome Res. 2003;2:556-7.
[42] Wang L, Yang W, Ju W, Wang P, Zhao X, Jenkins EC, et al. A proteomic study of Hutchinson-Gilford progeria syndrome: Application of 2D-chromotography in a premature aging disease. Biochem Biophys Res Commun. 2012;417:1119-26.
[43] Brown EJ, Beal PA, Keith CT, Chen J, Shin TB, Schreiber SL. Control of p70 s6 kinase by kinase activity of FRAP in vivo. Nature. 1995;377:441-6.
[44] Marino G, Ugalde AP, Salvador-Montoliu N, Varela I, Quiros PM, Cadinanos J, et al. Premature aging in mice activates a systemic metabolic response involving autophagy induction. Hum Mol Genet. 2008;17:2196-211.
[45] Cao K, Graziotto JJ, Blair CD, Mazzulli JR, Erdos MR, Krainc D, et al. Rapamycin reverses cellular phenotypes and enhances mutant protein clearance in Hutchinson-Gilford progeria syndrome cells. Sci Transl Med. 2011;3:89ra58.
[46] Viteri G, Chung YW, Stadtman ER. Effect of progerin on the accumulation of oxidized proteins in fibroblasts from Hutchinson Gilford progeria patients. Mech Ageing Dev. 2010;131:2-8.
[47] Villa-Bellosta R, Rivera-Torres J, Osorio FG, Acin-Perez R, Enriquez JA, Lopez-Otin C, et al. Defective extracellular pyrophosphate metabolism promotes vascular calcification in a mouse model of hutchinson-gilford progeria syndrome that is ameliorated on pyrophosphate treatment. Circulation. 2013;127:2442-51.
[48] Monsalve M, Borniquel S, Valle I, Lamas S. Mitochondrial dysfunction in human pathologies. Front Biosci. 2007;12:1131-53.
[49] Falutz J. Therapy insight: Body-shape changes and metabolic complications associated with HIV and highly active antiretroviral therapy. Nat Clin Pract Endocrinol Metab. 2007;3:651-61.
[50] Peinado JR, Quiros PM, Pulido MR, Marino G, Martinez-Chantar ML, Vazquez-Martinez R, et al. Proteomic profiling of adipose tissue from Zmpste24-/- mice, a model of lipodystrophy and premature aging, reveals major changes in mitochondrial function and vimentin processing. Molecular & cellular proteomics : MCP. 2011;10:M111 008094.
[51] Ahlqvist KJ, Hamalainen RH, Yatsuga S, Uutela M, Terzioglu M, Gotz A, et al. Somatic progenitor cell vulnerability to mitochondrial DNA mutagenesis underlies progeroid phenotypes in Polg mutator mice. Cell Metab. 2012;15:100-9.
[52] Fuster JJ, Andres V. Telomere biology and cardiovascular disease. Circ Res. 2006;99:1167-80.
[53] Blasco MA. Telomere length, stem cells and aging. Nature chemical biology. 2007;3:640-9.

[54] Sahin E, Colla S, Liesa M, Moslehi J, Muller FL, Guo M, et al. Telomere dysfunction induces metabolic and mitochondrial compromise. Nature. 2011;470:359-65.
[55] Allsopp RC, Vaziri H, Patterson C, Goldstein S, Younglai EV, Futcher AB, et al. Telomere length predicts replicative capacity of human fibroblasts. Proc Natl Acad Sci U S A. 1992;89:10114-8.
[56] Decker ML, Chavez E, Vulto I, Lansdorp PM. Telomere length in Hutchinson-Gilford progeria syndrome. Mech Ageing Dev. 2009;130:377-83.

610

611 **FIGURE LEGENDS**

612

613

614 **Figure 1**. **Study design and schematic overview of the results of analysis by SILAC.** Human
615 primary skin fibroblasts obtained from 2 healthy controls (8-year-old male and 13-year-old female)
616 and 2 HGPS patients (8-year-old male and 14-year-old female) were respectively grown in "heavy" or
617 "light" DMEM medium. After differential labeling, the female and the male HGPS cell lysates were
618 mixed with the female and male control cell lysates, respectively, and digested to a single pool of
619 peptides. The female HGPS-control and male HGPS-control pools were analyzed in duplicate by
620 liquid chromatography in tandem with mass spectrometry (LC-MS/MS), which allowed the
621 identification and quantification of 3,304 proteins. Among these, 536 proteins showing ≥1.5 fold
622 change and $p<0.01$ in both replicates of each female HGPS-control and male HGPS-control pool
623 comparison were classified as deregulated only in male HGPS vs. male control (Table S1), only in
624 female HGPS vs. female control (Table S2), and down- or up -regulated in both male and female
625 HGPS vs. control (Tables S3-S4 respectively).

626

627 **Figure 2. Mitochondrial function is impaired in HGPS skin fibroblasts.** (A) The cartoon shows
628 proteins deregulated in both male and female HGPS fibroblasts. Higher expression was found in
629 proteins related to metabolic energy pathways (red: PGK1, ENO2, PKM; LDH), and lower expression
630 in mitochondrial Complex V (green). Complexes, substrates and products of the mitochondrial
631 respiratory chain are also shown. (B) Western blot analysis showing markedly reduced levels of the
632 indicated mitochondrial proteins in HGPS fibroblasts (1:AG01972 and 2: AG06297) versus cells from
633 healthy controls (1:GM01651 and 2:GM08398). Actin was used as a loading control. (C)
634 Mitochondrial ATP synthesis measured in digitonin-permeabilized cells using a kinetic luminescence
635 assay. (D) Spectrophotometric determination of the activities of complex IV (COX) and citrate
636 synthase (CS), a Krebs cycle enzyme used to normalize COX activity (COX/CS). Enzyme activities
637 are expressed relative to control (=1). Data are means±SD from two independent experiments carried

638 out in triplicate. Data in C and D show the mean for the two cell lines of each genotype. Statistical
639 significance was determined by unpaired two-tailed t-test. **, $P < 0.01$; ***, $P < 0.001$.
640
641 **Figure 3. Mitochondrial function is impaired in skin fibroblasts from progeroid *Lmna*$^{G609G/G609G}$**
642 **and *Zmpste24*$^{-/-}$ mice.** Immortalized MAFs of the indicated phenotype were analyzed. Data are
643 means±SD of experiments performed in triplicate (A-C) or quadruplicate (D). (A) ATP production.
644 (B) COX and CS activity and COX/CS ratio. (C) Oxygen consumption. (D) Capacity of MAFs to
645 grow in medium containing galactose (Gal) or glucose (Glu) as the carbon source. Data show the ratio
646 of cell growth in Gal/Glu media measured in logarithmic relative fluorescence units (RFU). Results in
647 A, B and D are shown relative to wild-type (=1). Statistical significance was determined by one-way
648 ANOVA with Dunnett's post-hoc test. *, $P < 0.05$; ***, $P < 0.001$.
649
650 **Figure 4. Progerin and prelamin A expression is associated with mitochondrial dysfunction in**
651 **different tissues in a time- and dose-dependent manner.** COX and CS activities were measured in
652 tissues extracted from mice of the indicated genotypes (wild-type, *Lmna*$^{G609G/+}$, *Zmpste24*$^{-/-}$: n=5;
653 *Lmna*$^{G609G/G609G}$: n=4). Results are shown relative to wild-type (=1). (A) COX/CS ratio in hearts of 10-
654 and 32-week-old mice. (B) COX/CS ratio and western blot of skeletal muscle and brain extracts
655 prepared from 17-19-week-old mice. Antibodies against Lamin A/C were used to detect wild-type
656 lamin A and lamin C (white arrowheads) and prelamin A and progerin (black arrowheads). GAPDH
657 was used as loading control. (C) COX/CS ratio in hearts of 17-19-week-old-mice. Statistical
658 significance was assessed by one-way ANOVA with Dunnett's post-hoc test. WT versus mutant mice:
659 **, $P < 0.01$ and ***, $P < 0.001$; *Lmna*$^{G609G/G609G}$ versus *Lmna*$^{G609G/+}$: †, $P < 0.001$; 10-week-old versus
660 32-week-old *Lmna*$^{G609G/+}$: $^{\#}$, $P < 0.001$.
661
662 **Figure 5. Isoprenylation inhibitors improve mitochondrial function in progeroid cells.**
663 Immortalized MAFs of the indicated genotype were grown in the absence (mock) or presence of FTI-
664 277 (7 days) or a combination of pravastatin plus zoledronate (3 days). Mitochondrial function was
665 assessed by ATP synthesis and COX/CS ratio. Data are means±SD of three independent experiments

carried out in duplicate. All results are shown relative to wild-type mock (=1). Statistical significance was determined by one-way ANOVA with Dunnett's post-hoc test. For simplicity, only comparisons with mock of the same genotype are indicated: *, $P < 0.05$; **, $P < 0.01$. Consistent with the results of Figure 3, ATP synthesis and COX/CS ratios were significantly lower in mock progeroid cells than in mock wild-type cells ($P<0.001$).

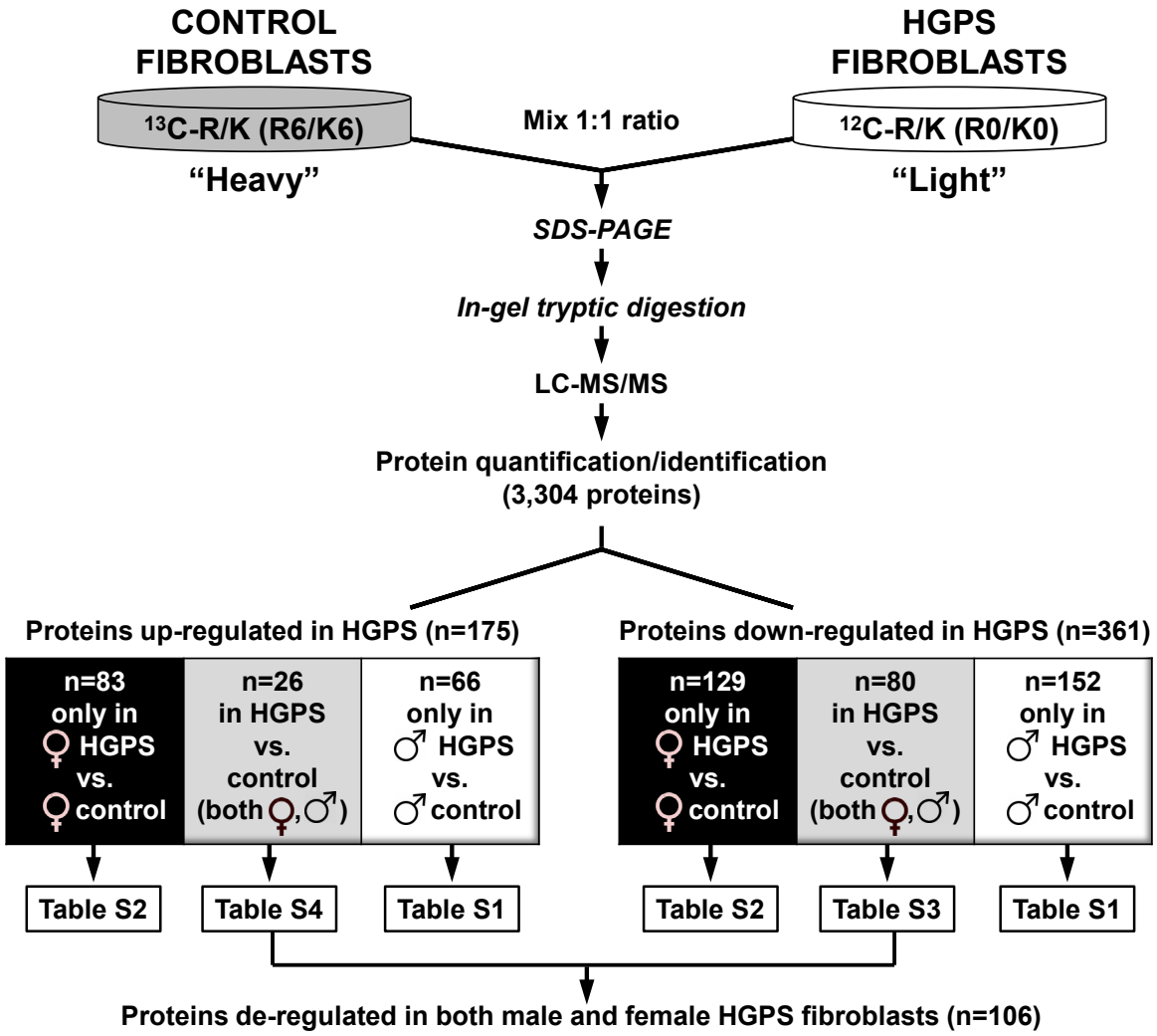
CONTROL FIBROBLASTS
HGPS FIBROBLASTS
13C-R/K (R6/K6)
Mix 1:1 ratio
12C-R/K (R0/K0)
"Heavy"
"Light"
SDS-PAGE
In-gel tryptic digestion
LC-MS/MS
Protein quantification/identification
(3,304 proteins)
Proteins up-regulated in HGPS (n=175)
Proteins down-regulated in HGPS (n=361)
n=83 only in ♀ HGPS vs. ♀ control
n=26 in HGPS vs. control (both ♀,♂)
n=66 only in ♂ HGPS vs. ♂ control
n=129 only in ♀ HGPS vs. ♀ control
n=80 in HGPS vs. control (both ♀,♂)
n=152 only in ♂ HGPS vs. ♂ control
Table S2
Table S4
Table S1
Table S2
Table S3
Table S1
Proteins de-regulated in both male and female HGPS fibroblasts (n=106)

FIGURE 1

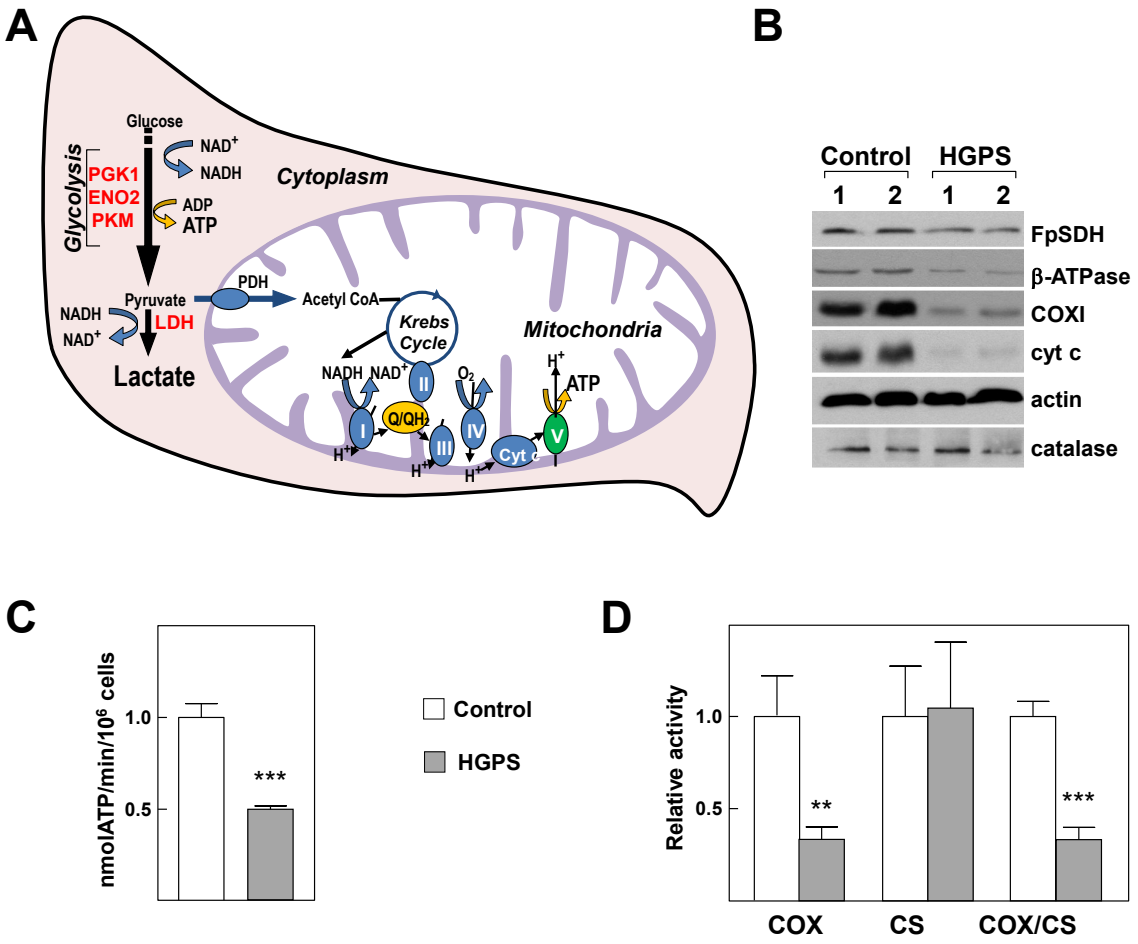
A
Glucose
NAD+
NADH
Glycolysis
PGK1
ENO2
PKM
ADP
ATP
Cytoplasm
PDH
Acetyl CoA
Krebs Cycle
Mitochondria
Pyruvate
NADH
NAD+
LDH
Lactate
NADH NAD+
II
O2
H+
ATP
I
Q/QH2
III
IV
V
Cyt c
B
Control
HGPS
1 2 1 2
FpSDH
β-ATPase
COXI
cyt c
actin
catalase
C
nmolATP/min/10^6 cells
1.0
0.5
***
Control
HGPS
D
Relative activity
1.0
0.5
**
***
COX
CS
COX/CS

FIGURE 2

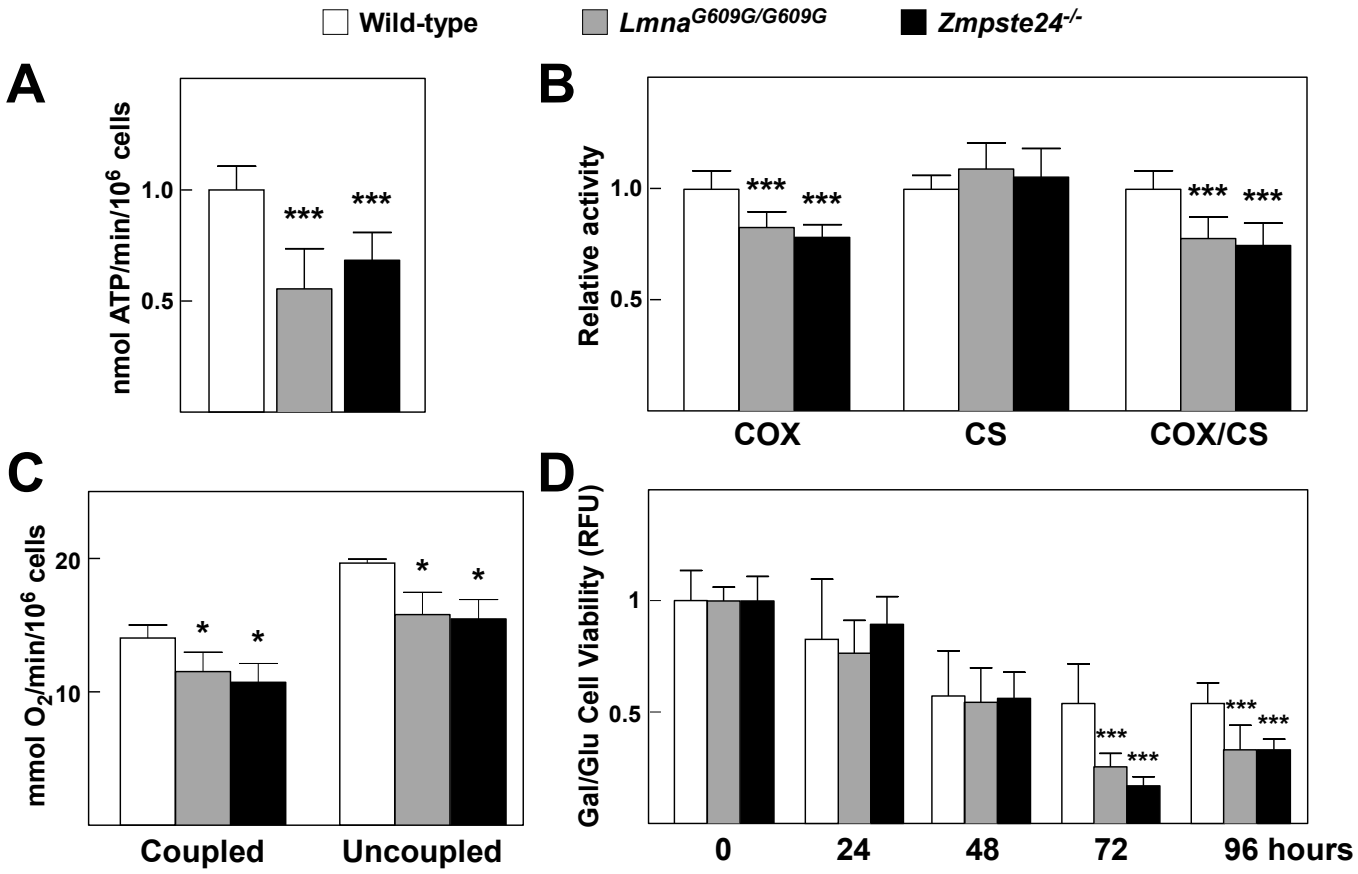
Wild-type
Lmna G609G/G609G
Zmpste24 -/-
A
nmol ATP/min/10 6 cells
1.0
0.5
***
***
B
Relative activity
1.0
0.5
***
***
***
***
COX
CS
COX/CS
C
mmol O2/min/10 6 cells
20
10
*
*
*
*
Coupled
Uncoupled
D
Gal/Glu Cell Viability (RFU)
1
0.5
***
***
***
***
0
24
48
72
96 hours

FIGURE 3

.

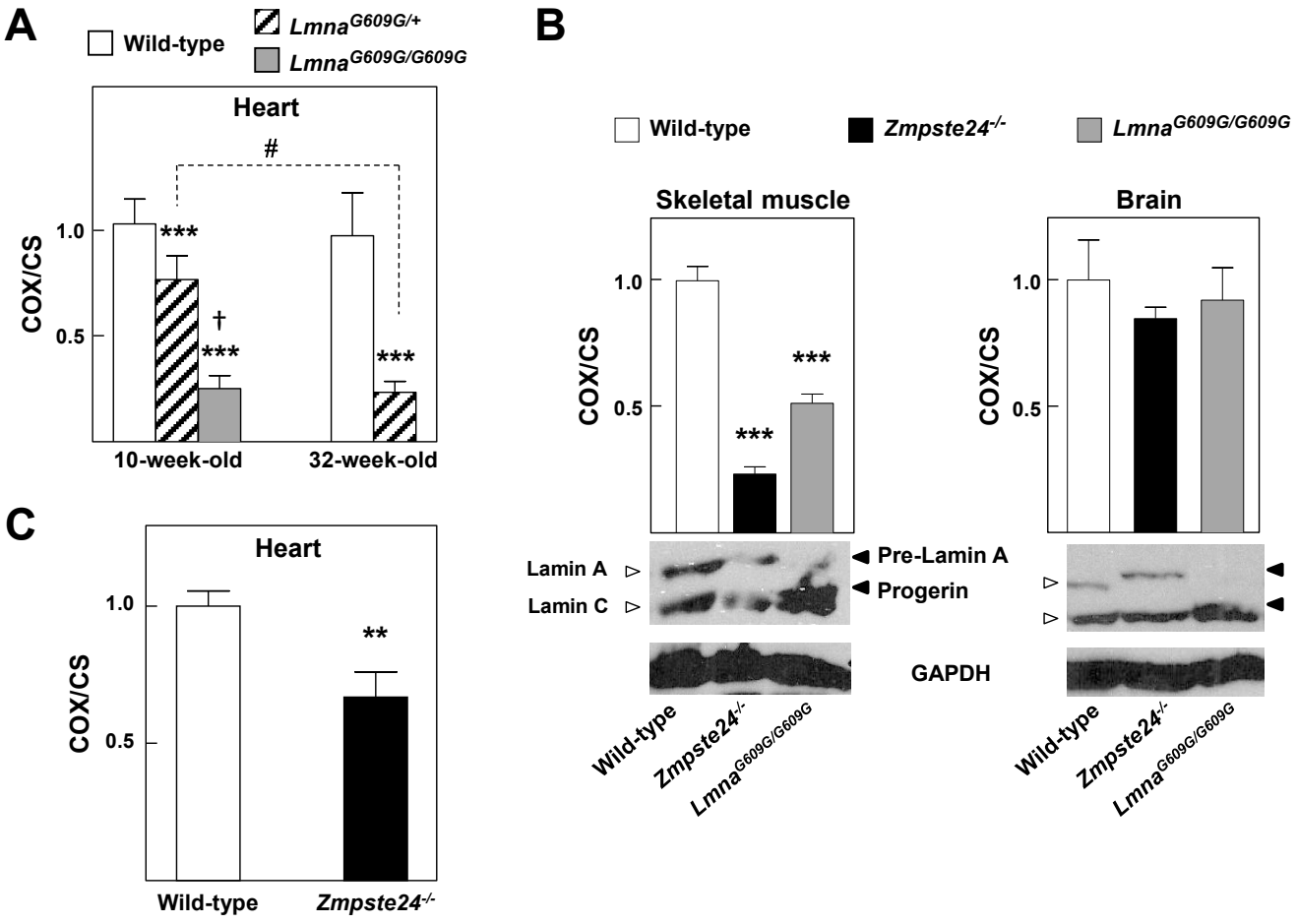
A
Wild-type
Lmna G609G/+
Lmna G609G/G609G
Heart
COX/CS
1.0
0.5
#
***
†
***
***
10-week-old
32-week-old
B
Wild-type
Zmpste24 -/-
Lmna G609G/G609G
Skeletal muscle
Brain
COX/CS
1.0
0.5
***
***
Lamin A
Lamin C
Pre-Lamin A
Progerin
GAPDH
Wild-type
Zmpste24 -/-
Lmna G609G/G609G
C
Heart
COX/CS
1.0
0.5
**
Wild-type
Zmpste24 -/-

FIGURE 4

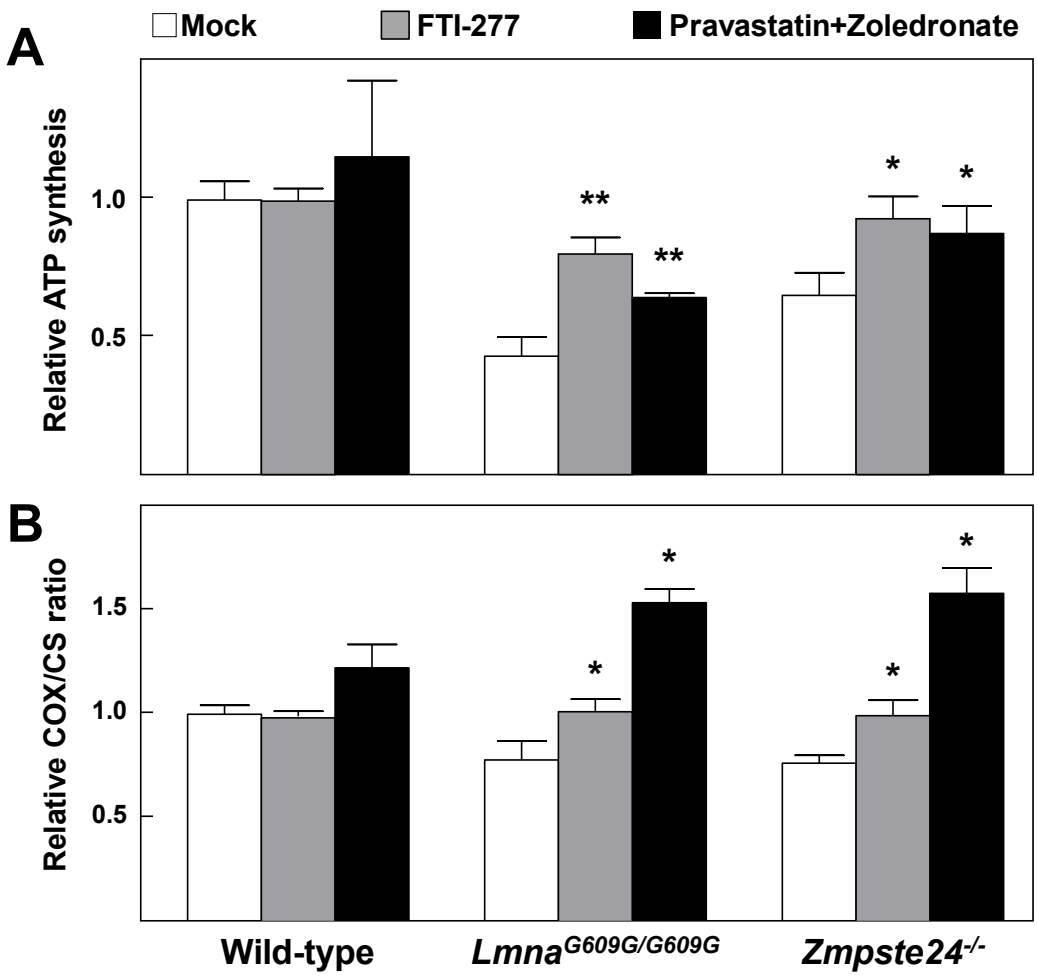
A
Mock
FTI-277
Pravastatin+Zoledronate
Relative ATP synthesis
1.0
0.5
**
**
*
*
B
Relative COX/CS ratio
1.5
1.0
0.5
*
*
*
*
Wild-type
Lmna G609G/G609G
Zmpste24 -/-

FIGURE 5